Flow Measurement and Instrumentation 91 (2023) 102341

Contents lists available at ScienceDirect

Flow Measurement and Instrumentation

journal homepage: www.elsevier.com/locate/flowmeasinst

River velocity measurements using optical flow algorithm and unoccupied aerial vehicles: A case study

Jamir Shariar Jyoti [a,*], Henry Medeiros [a,c,1], Spencer Sebo [b], Walter McDonald [b]

[a] Electrical and Computer Engineering, Marquette University, 1515 W. Wisconsin Ave, Milwaukee, WI, 53233, USA
[b] Construction and Environmental Engineering, Marquette University, 1637 W Wisconsin Ave, Milwaukee, WI, 53233, USA
[c] Agricultural and Biological Engineering, University of Florida, 1741 Museum Road, Gainesville, FL, 32611, USA

ARTICLE INFO

Keywords:
River velocimetry
Optical flow
Remote sensing
Aerial imaging

ABSTRACT

Accurate and reliable measurements of river flow are critical for a multitude of hydrologic engineering applications. However, flow rate measurements using in-situ sensors are uncertain in many applications and physical measurements of velocity may not be practical due to inaccessible sites or flood conditions. Recent advances in remote sensing using unoccupied aerial vehicles have overcome these limitations through non-contact measurements of river velocities; however, existing approaches have several shortcomings, including the need for artificial tracers in the absence of debris and prior knowledge of tracer size, shape, and flow direction. This case study seeks to overcome these shortcomings through the development of a system that utilizes drones, video imaging, and state-of-the-art optical flow algorithms to measure velocity in rivers. This system was applied along Menomonee River in Wauwatosa, WI. To remotely sense river flow, a DJI Matrice 210 RTK drone equipped with a Zenmuse X5S camera was used to capture video. The video data from the drone was analyzed using optical flow algorithms to generate velocity estimations. River velocity was measured directly at point locations using a hand-held velocimeter. Results indicate that the optical flow algorithms estimate the magnitude of surface velocity to within 13–27% of hand-held measurements without the use of artificial seeding. These outcomes suggest that this system could be used as a possible method to measure velocities in rivers.

1. Introduction

Measurements of river velocity are critical for developing engineering solutions to numerous hydrologic problems. For example, velocity is necessary for calibrating stage-discharge curves of continuous monitoring stations, understanding pollutant transport, and designing hydraulic channels. However, despite the widespread need for accurate and reliable measurements of river velocity, direct measurements of velocity can be challenging with existing methods that use in-situ approaches. This is because these methods can be unsafe to deploy in flood conditions due to extreme flood stage, high velocities, and large river debris. In addition, while there are many well established methods to measure velocity or discharge, e.g., acoustic doppler current profilers [1], current meters [2], and tracers [3], they may also exhibit significant errors associated with velocity estimations [4–6], especially during flood conditions [7]. Additionally, it is difficult to use these methods to measure river velocities in remote areas with inaccessible terrain. Given these challenges, new and alternative approaches are needed for collecting accurate, safe, and reliable river velocity data.

Cameras that can collect video of the flow from either fixed locations or from drones are an alternative non-intrusive technology that has potential to meet many of the challenges associated with existing velocity measurement methods. Fixed cameras can be mounted above the flow at locations that cross the river such as bridges; however, they rely on fixed locations and cannot be deployed on demand such as other boat-mounted acoustic doppler current profilers that are commonly used to develop flow rating curves for level-based flow monitoring stations. On the other hand, drones i.e., Unoccupied Aerial Vehicles (UAVs) have seen an emergence in hydrological applications, such as urban stormwater [8], ecohydrology [9], and hydro-morphology [10], due to their ability to collect data in high spatial resolution and at on demand time scales. Within hydrology, a recent application is the use of drones to

* Corresponding author.
E-mail addresses: jamirshariar.jyoti@marquette.edu (J.S. Jyoti), henry.medeiros@marquette.edu, hmedeiros@ufl.edu (H. Medeiros), spencer.sebo@marquette.edu (S. Sebo), walter.mcdonald@marquette.edu (W. McDonald).
[1] Part of this work was performed while Henry medeiros was with Marquette University.

https://doi.org/10.1016/j.flowmeasinst.2023.102341
Received 14 February 2021; Received in revised form 8 January 2023; Accepted 27 February 2023
Available online 10 March 2023
0955-5986/

measure surface velocity in rivers [11]. Image-based flow measurement techniques called Particle Image Velocimetry (PIV) and Large Scale Particle Image Velocimetry (LSPIV) have been successfully applied to drone videos of river flow to track the velocity of water [12–16]. These image-based methods estimate water velocities by using a pattern matching technique that measures the similarity of objects in two consecutive images using a similarity index using direct cross correlation or Fourier transforms [17]. That is, these methods generally partition the video frame into a grid and search the area within a region of interest around each grid cell in the next frame for the position that is most similar to its corresponding patch. The estimated displacement of each patch represents the flow velocity within the corresponding grid cell. They have shown promise to measure river velocity non-intrusively; however, these methods have practical limitations. One important limitation is the need for prior knowledge of the size and shape of the particles to be tracked on the surface of the river [18]. Therefore, this sometimes requires the introduction of synthetic or artificial floating material uniformly across the surface [19]. In some cases, such as in extreme floods or rivers with inaccessible terrain, external seeding or a prior knowledge of tracer size and shape may not be possible.

A potential alternative method to estimate velocity of river is optical flow, which is a computer vision algorithm that computes the displacement of pixels between two consecutive image frames. It represents the apparent motion of image objects between these frames caused by the movements of objects or camera [20]. Optical flow has been applied in numerous object tracking problems, including video segmentation [21,22], object tracking [23], vehicular traffic [24], surf foam [25], and human movement analysis [26], among others. Unlike PIV and LSPIV methods, optical flow does not compute the similarity between patches of subsequent video frames. Instead, it directly estimates the displacement of individual pixels regardless of the previous appearance of the image region surrounding them. Optical flow has also been demonstrated as an effective way to measure the velocity of fluid flows under experimental conditions [27,28]. This has led to the application of optical flow to images of rivers in order to estimate velocity [29,30] due to its potential to estimate velocity at higher spatial resolutions and without the need of tracers in the river. Specifically, optical flow can track the displacement of vectors caused by the velocity of water that transfers debris, bubbles, or waves in the direction of flow. Unlike other image-based methods, these can be monitored at a very-fine scale and therefore do not require larger particles to track. The result of the application of optical flow is a dense two-dimensional vector field where each vector represents the displacement of points in the river from one frame to the next. With a known pixel size and time between image frames, this displacement can then be converted into a velocity.

Due to these potential advantages, optical flow has been applied in case studies to measure the velocity of river flows, specifically through the application or adaptation of the Lukas-Kanade algorithm [18, 31–35]. While these case studies have shown promise, the Lukas-Kanade method is based on simplifying modelling assumptions that limit its applicability to low magnitude flows. More recent approaches employ machine learning strategies to learn an implicit optical flow representation based on observed video data [36–39]. These methods have consistently demonstrated state-of-the-art performance in most benchmark video datasets for optical flow evaluation [40,41–43]. Hence, machine learning approaches are currently the dominant strategy in the design of state-of-the-art optical flow estimation algorithms for computer vision applications; however, the application of these approaches for measuring river velocity is underexplored.

This study applies a machine learning approach for optical flow computation to videos of river flow to estimate surface velocity at a case study at a site on the Menomonee River in Wauwatosa, WI. At the case study location, we collected videos of river flow using a drone-mounted camera and applied an optical flow algorithm to develop an estimate of velocity across the entire flow surface. These estimations were then compared with ground-truth measurements of velocity using a hand-held velocity meter at discrete locations within the river. We also discuss the environmental and methodological parameters that influence the accuracy of the proposed method, such as lighting, wind speed, and camera resolution. Results suggest that this may be a viable alternative to other remote sensing methods that use image-based approaches to measure river velocity. In doing so, we present a fast, non-intrusive, remote method to measure river velocities.

2. Material and methods

2.1. Case study location

The case study location is a stretch of the Menomonee River in Wauwatosa, WI that drains a watershed of approximately 319 km^2 (Fig. 1). This area of the river is relatively shallow (<1.5 m), easy to access, and has available space nearby to take off and land the drone. At the monitoring location, the river is approximately 21 m wide and is characterized by a deeper (1–1.5 m) slow flow (upstream) followed by a shallow (0.3–0.6 m) more turbulent flow (downstream) with exposed rocks. Approximately 0.6 km upstream of this location is a USGS stream monitoring station (number 04087120). This station uses a stage-discharge relationship at the stream station to estimate discharge based upon measurements of water level [44].

Monitoring was conducted during three days in the summer and fall of 2019 (Table 1). Weather data, including rainfall, wind speed, wind direction, and solar radiation, was collected using a weather station located on the Marquette University Campus, which is situated approximately 7.5 km away from the data collection site. Flights A and B captured data at two elevations, while Flight C captured data at 11 different elevations. The flights captured a range of flow and environmental conditions, with wind speeds ranging from 2.7 to 8.6 m/s and a variation in cloud cover as indicated by the range in solar radiation. In addition, the flights captured a range of flow conditions from 1 to 30 m^3/s.

2.2. Data collection methods

Video of the river flow was collected using a DJI Matrice 210RTK drone. This drone has a real-time kinematic (RTK) GPS system that allows for centimeter-level positional accuracy through the combination of dual drone RTK antennas and a ground-based global navigation satellite system (GNSS) mobile station. Because of this GPS accuracy, the drone can hover steadily within ±0.1 m horizontally and vertically according to the manufacturer's specifications in typical environmental conditions [45], which were observed for all three flights. This is important for the accurate estimation of pixel size in the videos as it allows for data collection at steady elevations.

Video was collected from the drone with a gimbal-mounted Zenmuse X5S camera that filmed in 4096x2160 resolution at 30 frames per second. We determined the intrinsic camera parameters and lens radial distortion coefficients using the method proposed by Strobl and Hirzinger [46] and implemented in the publicly available OpenCV library (https://docs.opencv.org/master/d9/d0c/group_calib3d.html). A linear relationship was established between the camera distance to an object and the pixel size of the image using 100 images of a 623 × 534 mm black and white checkerboard pattern comprised of 6x9 squares of 87 mm, which were captured at distances between 0.5 m and 3.0 m from the camera. We verified the accuracy of the camera parameters by acquiring images of the calibration pattern at the same heights used for data acquisition and estimating the corresponding pixel sizes. To verify the drone's hovering accuracy reported by the manufacturer, we captured 490 video frames of the checkerboard pattern with the vehicle hovering at an elevation of 15 m and computed the standard deviation of the orientation and position of the pattern as observed by the drone's

Fig. 1. Map of monitoring location (left image) and image of the river monitoring location taken from a drone on 8/16/2019 with flow moving from right to left (right image); (Basemap source: ESRI).

Table 1
Flight details.

Flight	Flight date	Flight time	Avg. Stage (m)	Avg. Wind speed (m/s)	Avg. Solar radiation (kW)	72 h Antecedent rainfall (mm)	Elevations (m)	USGS station average flow rate (m^3/s)	USGS gage height (m)	No. of measurement points
A	5/10/2019	9:30 a.m.	0.95	2.7	0.24	16	46, 61	10.5	0.95	8
B	8/16/2019	10:00 a.m.	0.54	5.2	0.70	1.8	21, 27	1.04	0.54	13
C	9/13/2019	1:30 p.m.	1.46	8.6	0.56	71	6, 9, 12, 15, 18, 21, 24, 27, 30, 33, 45	30	1.44	14

camera. The average rotation error was 0.4° and the average positional error was 0.03 m. The higher rotation error was likely due to wind disturbances to the drone's orientation that could not be promptly compensated for by the gimbal. Once the camera parameters were established, drone video was collected at the elevations shown in Table 1 for a duration of approximately 30 s each.

After the flights, velocity data at the surface of the river was collected at various points (Table 1) within the river reach using a hand-held OTT MF Pro electromagnetic current meter. To capture velocity near the surface and reduce the effect that the depth of flow may have on the ratio of the measured velocity to surface velocity, we measured the velocity with the current meter at 0.15 m below the surface, which also satisfied the minimum operating depth of 0.03 m for the meter with the operator standing downstream and to the side of the meter. The OTT MF Pro meter has an accuracy of ±2% over the range of velocities we measured during this study. We placed the meter at each location and waited until readings stabilized before recording the velocity. The meter takes readings every 250 ms and we used an averaging time of 5 s. Within the river, the locations of the handheld velocity data were determined from their measured distance from benchmark locations on the bank of the river and verified from imagery captured by the drone and from a camera near the bank of the river. This hand-held velocity data, along with the location of collection, were cataloged within ESRI ArcGIS as a point shapefile. This data was used to directly compare the results of the optical flow algorithm with measurements from the hand-held meter.

2.3. Algorithm and data processing

Our proposed approach for surface velocity measurement (Table 2), similar to our previous work [47], uses a computer vision algorithm called optical flow.

The classical optical flow formulation is mainly based on two assumptions [20]: (1) brightness constancy, which assumes that the pixel intensities of an object between two consecutive frames do not change, and (2) spatial smoothness, which assumes that neighboring pixels tend to have similar motion.

Table 2
Algorithm for river velocity estimation.

Algorithm.	
	Input: Sequence of images $I_t, t = 1, 2, \ldots, n$.
	Output: Average distribution of flow magnitude $\bar{\rho}$ and phase (θ).
1:	**for** each consecutive image pair (I_t, I_{t+l}) **do**
2:	Compute flow field $\left(f_x, f_y, t\right)$, $(t = 1, 2, \ldots, n-1)$ from PWC-Net
3:	**end for**
4:	Obtain the cumulative flow $\left(F_x, F_y\right) = \sum_{t=1}^{n-1}(f_x, f_y, t)$
5:	Compute (ρ, θ) from $\left(f_x, f_y\right)$ using Eqs. (4) and (5).
6:	**for** each θ **do**
7:	**if** $\theta < 0$ **then**
8:	Compute unwrapped phase $\theta_u = \theta + 360$
9:	**end if**
10:	**end for**
11:	Calculate the average flow magnitude $\bar{\rho} = \rho/(n-1)$
12:	Convert magnitude $\bar{\rho}$ from pixels per second to meter per second using Eq. 6.

Consider a pixel with intensity $I(x, y, t)$, where x and y represent the spatial location of the pixel at time t. If the pixel moves by a distance (dx, dy) in the next frame after a time interval dt, then according to the brightness constancy assumption:

$$I(x+dx, y+dy, t+dt) = I(x, y, t) + \frac{\partial I}{\partial x}dx + \frac{\partial I}{\partial y}dy + \frac{\partial I}{\partial t}dt + H.O.T. \quad (1)$$

where $H.O.T.$ stands for the higher order terms. Assuming pixel intensity remains the same in the next frame, we can say that:

$$I(x+dx, y+dy, t+dt) = I(x, y, t) \tag{2}$$

Therefore, for a single point in a vector field, we can define its movement according to the following optical flow constraint equation:

$$\frac{\partial I}{\partial x}f_x + \frac{\partial I}{\partial y}f_y + \frac{\partial I}{\partial t} = 0 \tag{3}$$

where f_x and f_y represent the velocity of a point along the x and y directions, respectively.

In the classical formulation, Eq. (2) can be used to compute the flow field (f_x, f_y, t) at time, t. More recent methods have been developed for optical flow estimation based on deep neural networks [48]. There are several state-of-the-art algorithms to compute optical flow such as Flownet [36], Flownet2 [37], TVNet [38], and PWC-Net [39], among others. For this study, we used the PWC-Net network, which achieves state-of-the-art results on publicly available optical flow benchmark datasets such as Sintel [40], Middlebury [41], KITTI [43], HD1K [42]. Furthermore, PWC-Net's low computational requirements allow us to process each image frame faster than the camera frame rate, which would enable real-time analysis of the data. In this study, we use the PWC-Net model pre-trained on the aforementioned datasets. That is, no additional training data or manual annotations are used to train the network.

The video data were collected in 4096x2160 resolution; however, PWC-Net is a neural network that was trained on images of one quarter of that resolution. Rather than training a larger model using upsampled versions of the training datasets, we resample the regions of interest within each video to a 1024x540 resolution video so they can be processed by the pre-trained, unmodified model. To avoid boundary artifacts caused by computing the optical flow near the image borders, our region of interest encompasses an area within and beyond the region where the ground truth flow is measured. PWC-Net takes consecutive image frames of the river flow video as input and outputs the corresponding optical flow field, (f_x, f_y, t). From the optical flow data generated on each image pair by PWC-Net, we remove outliers. Since the resolution of the region of interest and the camera frame rate are fixed, displacements in pixels per frame have a constant linear relationship with displacement in meters per second, which allows us to perform outlier removal using flow magnitudes measured in pixels (i.e., flows with magnitude lower than 1 pixel per frame and larger than 100 pixels per frame). We compute the cumulative flow field (F_x, F_y) in Cartesian coordinates (step 4 in Table 2) for the whole video by adding the Cartesian flow field of each image pair. We then convert the cumulative flow to polar coordinate values to generate the cumulative flow magnitude (ρ) and phase (θ) according to:

$$\rho = \sqrt{{F_x}^2 + {F_y}^2} \tag{4}$$

$$\theta = tan^{-1}\left(\frac{F_y}{F_x}\right) \tag{5}$$

The phase (θ) in Equation (5) is wrapped at this point, which means that it is constrained between $-180^\circ < \theta < 180^\circ$ and hence can show discontinuities at angles near the endpoints of this range. Phase unwrapping provides a true azimuth in the direction of the river and is performed in steps 6–10 in Table 2. The average flow magnitude ($\overline{\rho}$) is given by the cumulative magnitude divided by the number of video frame pairs (step 11 in Table 2). The average magnitude ($\overline{\rho}$) represents the velocity of the flow in pixels per frame. We finally convert this magnitude to meters per second ($\overline{\rho}_{mps}$) according to

$$\overline{\rho}_{mps} = \overline{\rho} * p_s * f_r \tag{6}$$

where p_s is the size of a pixel in meters and f_r is the frame rate of the video in frames per second (step 12 in Table 2). From the average of the distribution of the magnitude ($\overline{\rho}$) and the unwrapped phase (θ_u) over the processed video segment, we generate the histograms and heat maps of both magnitude and phase for qualitative and quantitative analysis. Our quantitative analysis is based on the mean, median, and mode values of the histograms over the flow region.

2.4. Comparing drone and hand-held velocities

Vector fields of velocity from PWC-Net were converted into a raster dataset by providing the size of each pixel and the latitude and longitude of the origin in degrees (i.e., lower left corner of the lower left cell). Hand-held velocities were georeferenced into ArcGIS as point shapefiles using measured distances from control points on the bank of the river. A buffer of 30 cm was created around each hand-held data collection point and the average value of the velocity field from PWC-Net within each buffer was computed using zonal statistics. This provided us with an estimation of velocity from the optical flow algorithm at each hand-held data collection location. We then computed the error as the difference between the hand-held velocity and the velocities estimated using optical flow at each point.

3. Results and discussion

3.1. Optical flow algorithm results

The videos collected by the drone were analyzed and velocities were found to be within 13–27% of the hand-held measurements. An example of the results from the video analysis is illustrated in Fig. 2 for Flight C at a 12-m elevation (results for the remaining flights are discussed in Section 3.3). In this video, the optical flow algorithm is tracking the velocity of surface particles, including waves, foam, and debris. During this video, the average hand-held velocity was 1.38 m/s with a phase of about 180°, indicating flow moving from right to left. Fig. 2(a) shows a single image from the video. We performed the analysis on a 15-s video clip and averaged the results. Fig. 2(b) represents the average magnitude heatmap, and the average magnitude histogram is depicted in Fig. 2(c). From the magnitude histogram, we can see that the mode of the velocity is 1.37 m/s.

The mean variance over the video is 0.046 $(m/s)^2$ and the maximum is 0.076 $(m/s)^2$. From the average phase histogram in Fig. 2(d), we can see that the phase is almost constant at approximately 180°, which is in the downstream direction.

We also measured the average processing time per frame for each step of our algorithm on a workstation equipped with an Intel® Core™ i5-8250U CPU @ 1.60 GHz and four NVIDIA RTX 2080 Ti GPUs. Optical flow computation is performed on one of the GPUs whereas the remaining steps of the algorithm are computed using the CPU. Table 3 shows the average processing time per frame for each step of our algorithm and its corresponding standard deviations. Given the overall mean computation time of 38.75 ms, it is possible to process the videos at a rate of approximately 25.7 frames per second using a single GPU and without resorting to CPU parallelization strategies. Since there are no data dependencies among the video frames, all the steps of the algorithm can be executed in parallel, leading to an average rate of 102.8 frames per second in our workstation equipped with four GPUs. These results show that it is possible to process the video frames as they are acquired. Developing a system to transmit the frames to a remote computer and process them in real-time is part of our future work.

The camera's focal distance was found to be approximately 4181.5 pixels (4182 and 4181 along the vertical and horizontal image axes, respectively). Since we resample our region of interest (ROI) to have a constant resolution of 1024x540 pixels, the corresponding pixel size is 8.9 mm, regardless of the elevation of the drone. Pixel size is computed using a pinhole camera model. Hence, maintaining a constant resolution is equivalent to keeping a constant ratio between the focal length of the camera and the elevation of the drone [49]. The maximum pixel error caused by radial distortion within the ROI is 1.51 mm. As Fig. 3

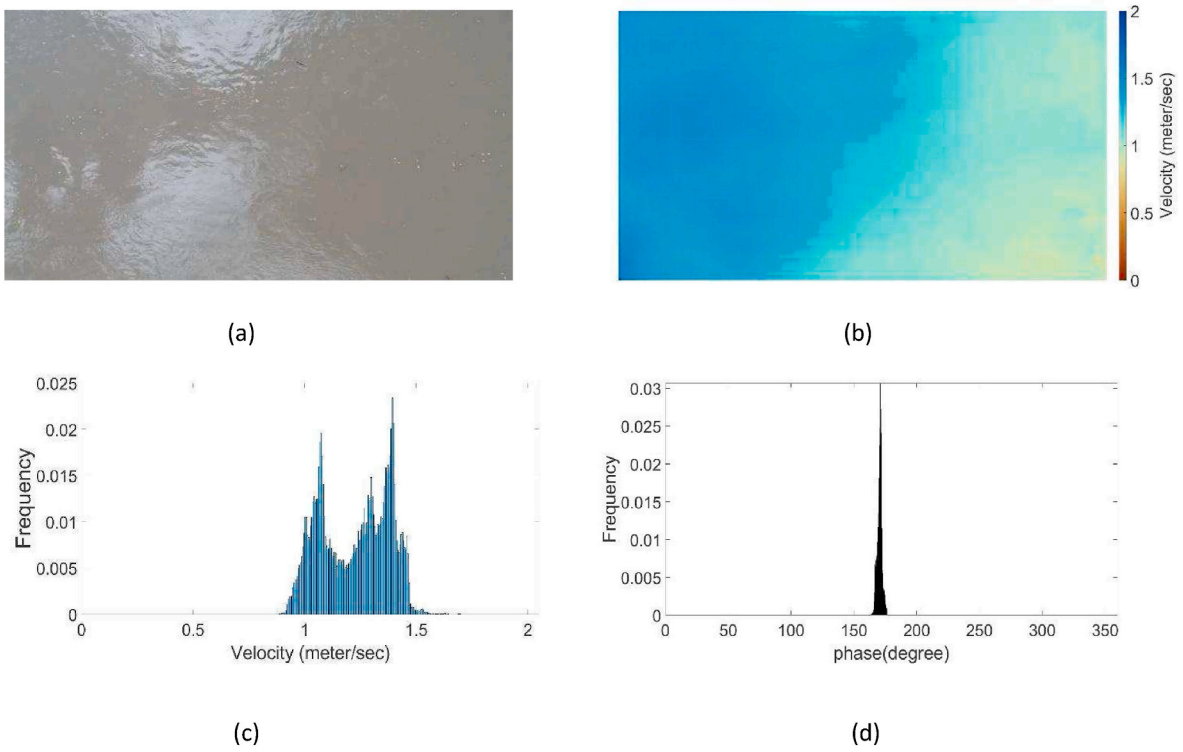

Fig. 2. Illustration of the results generated by our method (a) an image from the video (b) magnitude heatmap (c) magnitude histogram (d) phase histogram.

Table 3
Mean and standard deviation of the computation time for each step of the algorithm.

Step	Mean (ms)	Std dev. (ms)
Rescale image	0.15	0.05
Compute optical flow	28.80	0.68
Outlier removal	1.95	0.22
Compute mean polar flow	7.85	4.52
Total	**38.75**	**5.47**

indicates, the impact of radial distortion within the ROI is minimal. Hence, to simplify the overall framework, we do not perform radial distortion correction in the video frames.

3.2. Impact of resolution and brightness on optical flow

The elevation at which the drone is flown has a direct impact on the distance that each pixel represents in space. For example, for the camera used in our experiments, at a 45 m elevation, the pixel size is 1.1 cm, whereas at 100 m, the corresponding pixel size is approximately 2.7 cm. There may be instances therefore in which the algorithm is unable to detect movement in pixels due to a combination of a large pixel size and a low flow velocity. Conversely, there may be instances in which pixel size is small and velocity is high, resulting in such a high pixel displacement that the optical flow algorithm cannot capture it. We therefore evaluated the relationship between the performance of the algorithm and the average pixel displacement (i.e., velocity). In addition, we explored methods to overcome limitations of pixel displacements through resampling the video resolution.

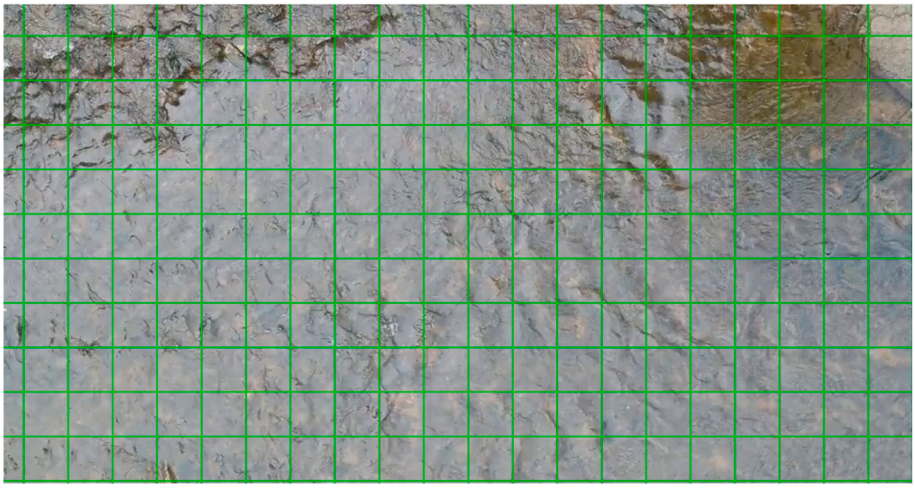

Fig. 3. Region of interest after radial distortion correction with overlaid grid to visualize the impact of radial distortion.

An example of the effects of resampling videos is illustrated in Fig. 4. Fig. 4(a), (b), and 4(c) represent the velocity of river flow from a common region of interest observed from different elevations that have original resolutions of 1600x1600, 656x656 and 416x416, respectively. From these three figures, it is clear that as the resolution of the video decreases, the algorithm is unable to detect movement within the river. This is because the low-resolution videos have pixel sizes that are too large to identify visual features in the image, needed to detect movement in the flow and because the displacement of these features between two consecutive frames may be smaller than the pixel size. To overcome this challenge, we increased the resolution of the videos in Fig. 4 (b) and 4 (c) to 1600x1600 by upsampling them using bilinear interpolation. By increasing the video resolution, the algorithm is able to recover most of the pixel displacement information and detect movement in the surface of the river as depicted in Fig. 4 (d) and 4 (e). These upsampled results are noticeably more similar to the high-resolution results in Fig. 4 (a) than the corresponding lower resolution videos in Fig. 4 (b) and 4 (c). Therefore, these results suggest that for videos with low pixel displacement either due to low video resolution, low stream velocity, or a combination, upsampling of the video may be used to improve algorithm performance.

As the working principle behind optical flow is based on the brightness constancy assumption, variations in video brightness may play an important role in the flow field analysis. In a preliminary analysis, we have observed a small variability in the flow estimation results as illumination changes. Fig. 5 illustrates the analysis of two different videos captured within the same flight. The image in Fig. 5(a) is from a video captured during cloud cover and the image in Fig. 5(b) is captured during a period of direct sunlight with no cloud cover. As illustrated in Fig. 5(c) and (d), as the brightness of the video increases, some of the flow magnitude information is lost in regions of higher reflectance, which is consistent with other studies that have found that reflectance from direct sunlight can produce errors in velocity measurements [50]. This is an important consideration in the application of this approach, as it is clear that brightness and/or shadows may influence the accuracy of the algorithm. As such, quantifying and mitigating the impact of illumination changes would be important for future work.

3.3. Comparison with ground truth velocities

The hand-held velocity monitoring locations were georeferenced within ArcGIS for comparison with the velocity data estimated from the drone video. An example of the measurement locations of the hand-held meter and the corresponding velocities estimated using the drone videos are shown in Fig. 6 for Flight C. For each flight, these measurement locations were different depending upon environmental conditions. For example, during Flight C, the flow within the middle of the river was above chest height, and therefore we were unable to obtain velocity data across the entire channel. However, during Flight B, the maximum depth was less than 1 m and therefore we were able to collect hand-held data across a larger area of the river.

A direct comparison of the hand-held velocity versus the drone velocity at the test points for Flights A, B, and C is illustrated in Fig. 7. In the figure, each point corresponds to the flow observed in one of the regions highlighted in Fig. 6 (for Flight C) averaged over all the flight altitudes listed in Table 1. The drone-measured velocities were within 15%, 27%, and 13% of the hand-held measurements on average for Flights A, B, and C, respectively. The drone estimations are consistently

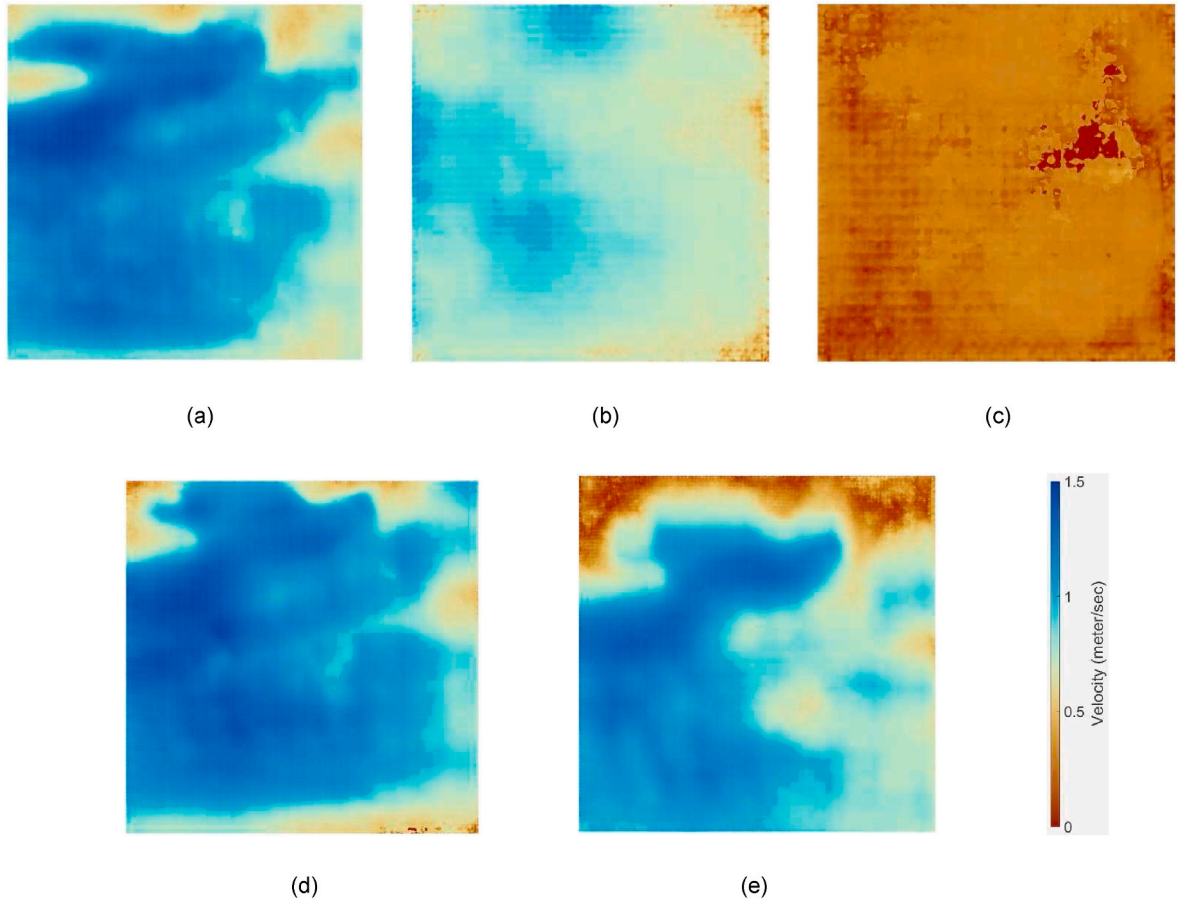

Fig. 4. Illustration of the impact of resolution in the estimation of optical flow. (a)–(c) Original videos at three elevations whose corresponding region of interest resolution is 1600x1600, 656x656 and 416x416, respectively. (d)–(e) Results corresponding to (b) and (c) after upsampling the region of interest to 1600x1600.

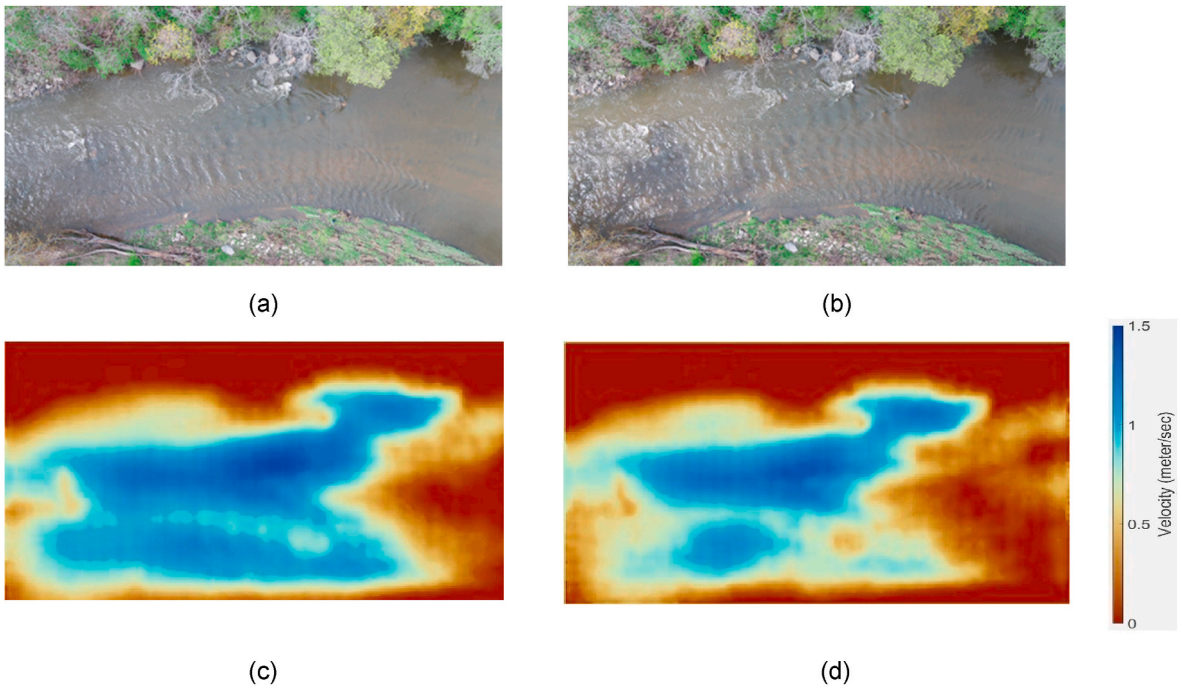

Fig. 5. Impact of illumination changes in flow estimation between videos collected 1 min apart. (a) Region of interest with low illumination (b) ROI with high illumination, (c), (d) flow magnitude heatmaps of (a) and (b), respectively.

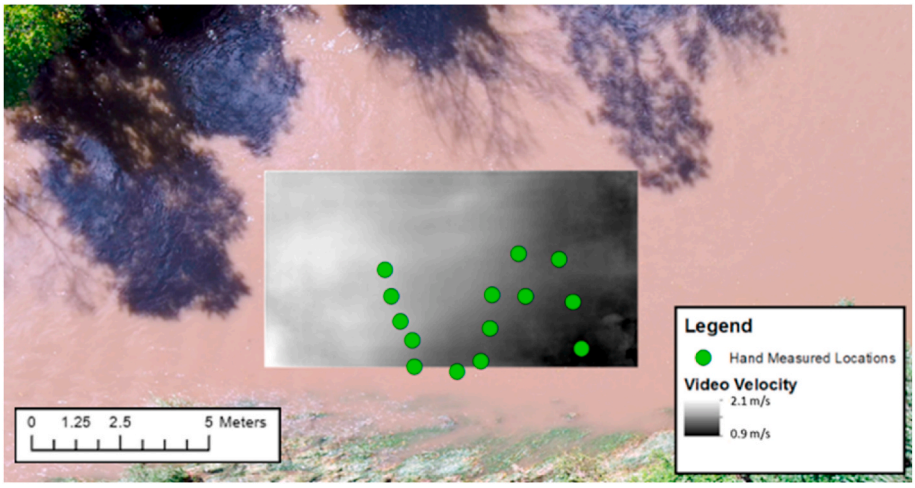

Fig. 6. Location of hand-held velocity measurements and depiction of velocities derived from drone video for Flight C.

lower than those from the hand-held device. This is similar to other studies that have found drone-estimated measurements using LSPIV to be less than in-situ measurements of velocity [15]. The variation in accuracy may be due to several factors including measurement uncertainty in the hand-held velocity meter, the proposed image analysis workflow, or the pixel displacement of the videos at different velocities. Since pixel displacement is a function of the actual flow velocity, under similar conditions, we expect flights with lower average flow velocity to show higher error due to displacements in the flow that are similar in size or smaller than the pixels themselves. This is directly observed in our datasets as the average velocities measured using the hand-held meter for Flights A, B, and C were 1.23 m/s (15% error), 0.54 m/s (27% error), and 1.38 m/s (13% error), respectively. This indicates a clear relation between the errors and the corresponding velocities.

To further explore how pixel displacements influence the error within our data, we plotted the percent error for each point against the pixel displacement of that point in Fig. 8. As illustrated for Dataset B, it appears that as the pixel displacement decreases and approaches one, the corresponding error increases as well. This suggests that there is a lower pixel displacement threshold impacted by the velocity of the water, resolution of the camera, and elevation of the flight for which the algorithm is unable to capture the velocity of the river. Hence, camera resolution and focal length, as well as the altitude of the drone during video capture must be specified based on the expected minimum flow that must be measured. Upsampling the images as described in Section 3.2 would extend the range of flow magnitudes that can be measured using the same camera without requiring dramatic changes in altitude.

As a whole, the average accuracy of our study across all flights as illustrated in Fig. 7 is 18%. This error is comparable to that of other particle tracking velocimetry studies using drone video that have found drone measurements to be within 16–31% of in-stream velocity measurements [15,34]. An advantage to our method is that it does not

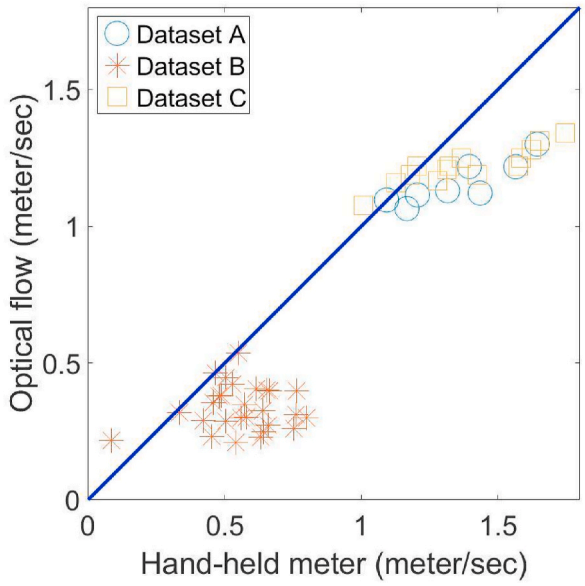

Fig. 7. Comparison of velocity data from hand-held meter and drone-derived velocities from various points measured in the river, where the blue line is a 1:1 line.

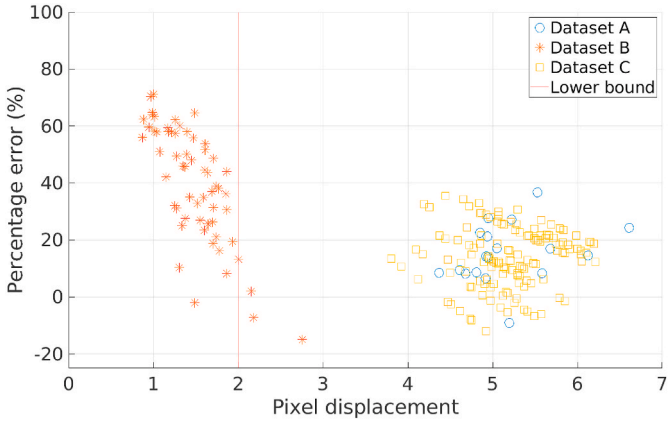

Fig. 8. Percentage flow velocity estimation error as a function of average pixel displacement.

require prior knowledge of particle size, shape, or direction, which makes its application advantageous in scenarios where this information may not be known. Therefore, the method presented in this paper may be a viable alternative to remotely measure river velocity without the need for seeding of the river.

3.4. Discussion of results

In this study, we applied an optical flow algorithm to videos of river flow to estimate surface velocities. Results from three flights at a river in Wauwatosa, WI indicated that our approach estimated velocities within 13–27% of hand-held measurements. The outcomes from this study suggest that the proposed approach using drone video and optical flow algorithms could be a useful tool for measuring surface velocities of rivers. An advantage of this approach over in-situ methods is that it does not require intrusive measurements of flow rates, which is helpful in inaccessible locations or during extreme floods. In addition, it does not require external seeding of the river, which may not be possible in scenarios where physical or environmental conditions limit the introduction of uniform seeding across a river.

While our study demonstrated the potential of this approach for measuring surface velocity in rivers, there were several limitations. These limitations include the need for adequate resolution in videos that the optical flow algorithm analyzes so that it can properly detect pixel movement. As demonstrated, resolutions in which pixel displacement is above two pixels provided the most accurate estimates of velocity. This pixel displacement is dependent upon the magnitude of the velocity in the river, the resolution of the camera, and the elevation of the drone. Another limitation is the influence of glare on the river during bright conditions; therefore, this approach may not be optimal under sunlight conditions in which there is significant glare. This limitation is consistent with similar studies where ambient light conditions influence the ability to estimate water quality constituents based upon drone imagery [51], which indicates it may be a limitation of remote sensing of surface waters using aerial images in general.

In addition, there are limitations of this method that may preclude its ability to measure river flow in certain applications. While the DJI Matrice 210 RTK can safely fly in rainfall conditions, many drones cannot; additionally, the camera on the drone may be damaged if it gets wet. Flights during rainfall events are therefore not possible. In addition, weather conditions in which there is heavy fog may prevent the capture of video of the river. Finally, many quadcopter drones such as the one used in this study are limited to flights in winds up to 12 m/s. However, even at high wind speeds that are within the manufacturer's specifications, instability of the drone may result in significant movement of the camera, which could impact the results of the algorithm.

Our approach was not tested during extreme flood conditions; however, there are several reasons why we believe that it could be a useful tool in those scenarios. During extreme conditions, the level of waves, bubbles, and floating debris will be higher, which would allow for easier detection of object movement. In addition, the pixel displacement at high speeds could be detected at lower spatial resolutions thereby reducing errors due to low pixel movement that were demonstrated in our study. This would also allow for the collection of videos at higher elevations, which would improve the field of view of the camera. However, there are other practical limitations that would restrict the use of drones in general during extreme floods including high wind speeds or heavy precipitation. Higher wind speeds are known to cause stability issues that influence accuracy of velocity measurements using LSPIV [52], and heavy precipitation precludes flying most drones. However, mitigating the impact of drone stability on data collection might be possible using data from the drone's inertial measurement unit. Investigating such strategies is part of our future work.

Our results suggest that the proposed method may be a viable alternative to other remote sensing methods that use an image-based approach to measure river velocity. Future work could include the application of the method under different flow regimes, such as high, low, or turbulent flows, or under alternative environmental conditions, such as lighting and wind speed. It could also include the direct comparison of our methodology with other types of optical flow or particle tracking velocity methods. In addition, other types of imaging, such as thermal imagery that have been shown to be effective for particle velocimetry [53], may provide more accurate representations of vector movement that could be advantageous for our proposed method. While this case study provides a first look at the application of optical flow for measuring surface velocity of rivers, the results demonstrate that this may be a fast, non-intrusive, remote method to measure river velocities.

4. Conclusions

In this paper, we present a technique for river velocity estimation using an optical flow algorithm applied to videos captured by drones. Results indicate that drone-derived velocities are within 13–27% of velocities measured by hand-held meters. While the results show promise, more research is needed to evaluate the impact of other environmental variables, such as lighting, river velocities, debris, and drone

instability from high winds, on system performance. However, these preliminary results demonstrate that optical flow methods may be effective at estimating river velocities from drone videos. This could provide a valuable alternative to in-stream monitoring systems for estimating river velocities during extreme flood conditions or in areas that are not easily accessible for in-situ measurements.

Credit author statement

Jamir Shariar Jyoti: Software implementation, Data collection and analysis, Writing. Henry Medeiros: Conceptualization, Methodology, Writing, Reviewing. Spencer Sebo: Data collection and analysis, Writing, Reviewing. Walter McDonald: Conceptualization, Methodology, Writing, Reviewing.

Declaration of competing interest

The authors declare the following financial interests/personal relationships which may be considered as potential competing interests: This work was funded by the generous support of the GHR seed grant through the Opus College of Engineering.

Data availability

Data will be made available on request.

Acknowledgements

This work was funded by the generous support of the GHR seed grant through the Opus College of Engineering.

References

[1] K. Oberg, D.S. Mueller, Validation of streamflow measurements made with acoustic Doppler current profilers, J. Hydraul. Eng. 133 (12) (2007) 1421–1432.
[2] A. Tazioli, Experimental methods for river discharge measurements: comparison among tracers and current meter, Hydrol. Sci. J. 56 (7) (2011) 1314–1324.
[3] D.P. Turnipseed, V.B. Sauer, Discharge measurements at gaging stations: U.S. Geological Survey Techniques and Methods book 3, chap. A8, 87 pp. (Also available at: https://pubs.usgs.gov/tm/tm3-a8/, 2010.
[4] M.F. Aguilar, W.M. McDonald, R.L. Dymond, Benchmarking laboratory observation uncertainty for in-pipe storm sewer discharge measurements, Journal of hydrology 534 (2016) 73–86.
[5] J. Le Coz, B. Camenen, X. Peyrard, G. Dramais, Uncertainty in open-channel discharges measured with the velocity–area method, Flow Meas. Instrum. 26 (2012) 18–29.
[6] R.D. Harmel, R.J. Cooper, R.M. Slade, R.L. Haney, J.G. Arnold, Cumulative uncertainty in measured streamflow and water quality data for small watersheds, Transactions of the ASABE 49 (3) (2006) 689–701, https://doi.org/10.13031/2013.20488.
[7] G.D. Baldassarre, A. Montanari, Uncertainty in river discharge observations: a quantitative analysis, Hydrol. Earth Syst. Sci. 13 (6) (2009) 913–921.
[8] W. McDonald, Drones in urban stormwater management: a review and future perspectives, Urban Water J. 16 (7) (2019) 505–518.
[9] E.R. Vivoni, A. Rango, C.A. Anderson, N.A. Pierini, A.P. Schreiner-McGraw, S. Saripalli, A.S. Laliberte, Ecohydrology with unmanned aerial vehicles, Ecosphere 5 (10) (2014) art130, https://doi.org/10.1890/ES14-00217.1.
[10] A.S. Woodget, R. Austrums, I.P. Maddock, E. Habit, Drones and digital photogrammetry: from classifications to continuums for monitoring river habitat and hydromorphology, Wiley Interdisciplinary Reviews: Water 4 (4) (2017) e1222, https://doi.org/10.1002/wat2.1222.
[11] M.T. Perks, S.F. Dal Sasso, A. Hauet, E. Jamieson, J. Le Coz, S. Pearce, S. Manfreda, Towards harmonisation of image velocimetry techniques for river surface velocity observations, Earth Syst. Sci. Data 12 (3) (2020) 1545–1559, https://doi.org/10.5194/essd-12-1545-2020.
[12] D. Strelnikova, G. Paulus, S. Käfer, K.H. Anders, P. Mayr, H. Mader, U. Scherling, R. Schneeberger, Drone-based optical measurements of heterogeneous surface velocity fields around fish passages at hydropower dams, Rem. Sens. 12 (3) (2020) 384.
[13] M. Bolognesi, G. Farina, S. Alvisi, M. Franchini, A. Pellegrinelli, P. Russo, Measurement of surface velocity in open channels using a lightweight remotely piloted aircraft system, Geomatics, Nat. Hazards Risk 8 (2017) 73–86.
[14] Q.W. Lewis, E.M. Lindroth, B.L. Rhoads, Integrating unmanned aerial systems and LSPIV for rapid, cost-effective stream gauging, J. Hydrol. 560 (2018) 230–246.
[15] F. Tauro, M. Porfiri, S. Grimaldi, Surface flow measurements from drones, J. Hydrol. 540 (2016) 240–245.
[16] F. Tauro, A. Petroselli, E. Arcangeletti, Assessment of drone-based surface flow observations, Hydrol. Process. 30 (2016) 1114–1130.
[17] M. Muste, I. Fujita, A. Hauet, Large-scale particle image velocimetry for measurements in riverine environments, Water Resour. Res. 44 (4) (2008).
[18] S. Pearce, R. Ljubičić, S. Peña-Haro, M. Perks, F. Tauro, A. Pizarro, S. Manfreda, An evaluation of image velocimetry techniques under low flow conditions and high seeding densities using unmanned aerial systems, Rem. Sens. 12 (2) (2020) 232.
[19] A. Pizarro, S.F. Dal Sasso, M.T. Perks, S. Manfreda, Spatial distribution of tracers for optical sensing of stream surface flow, Hydrol. Earth Syst. Sci. Discuss. Rev. (2020).
[20] B.K. Horn, B.G. Schunck, Determining Optical Flow. In Techniques and Applications of Image Understanding vol. 281, *Inter*national Society for Optics and Photonics, 1981, November, pp. 319–331.
[21] Y.H. Tsai, M.H. Yang, M.J. Black, Video segmentation via object flow, Proceedings of the IEEE conference on computer vision and pattern recognition (2016) 3899–3908.
[22] S.D. Jain, B. Xiong, K. Grauman, Fusionseg: learning to combine motion and appearance for fully automatic segmentation of generic objects in videos, in: IEEE Conference on Com*puter Vision and Pattern Recognition (CVPR)*, vol. 2017, IEEE, 2017, July, pp. 2117–2126.
[23] K. Kale, S. Pawar, P. Dhulekar, Moving object tracking using optical flow and motion vector estimation, in: 2015 4th International Conference *on Reliability, Infocom Technologies and Optimization (ICRITO)(trends and Future Directions*, IEEE, 2015, September, pp. 1–6.
[24] S. Aslani, H. Mahdavi-Nasab, Optical flow based moving object detection and tracking for traffic surveillance, International Journal of Electrical, Computer, Energetic, Electronic and Communication Engineering 7 (9) (2013) 1252–1256.
[25] P. Dérian, R. Almar, Wavelet-based optical flow estimation of instant surface currents from shore-based and UAV videos, IEEE Trans. Geosci. Rem. Sens. 55 (10) (2017) 5790–5797.
[26] K.F. Sim, K. Sundaraj, Human motion tracking of athlete using optical flow & artificial markers, in: International Conferen*ce on Intelligent And Advanced Systems*, vol. 2010, IEEE, 2010, June, pp. 1–4.
[27] T. Corpetti, D. Heitz, G. Arroyo, E. Mémin, A. Santa-Cruz, Fluid experimental flow estimation based on an optical-flow scheme, Exp. Fluid 40 (1) (2006) 80–97.
[28] D. Heitz, E. Mémin, C. Schnörr, Variational fluid flow measurements from image sequences: synopsis and perspectives, Exp. Fluid 48 (3) (2010) 369–393.
[29] M. Khalid, L. Pénard, E. Mémin, Application of optical flow for river velocimetry, in: IEEE International Geo*science and Remote Sensing Symposium (IGARSS)*, vol. 2017, IEEE, 2017, July, pp. 6243–6246.
[30] K. Bacharidis, K. Moirogiorgou, I.A. Sibetheros, A.E. Savakis, M. Zervakis, River flow estimation using video data, In2014 IEEE International Confere*nce on Imaging Systems and Techniques (IST) Proceedings* (2014, October) 173–178.
[31] M.T. Perks, A.J. Russell, A.R. Large, Advances in flash flood monitoring using unmanned aerial vehicles (UAVs), Hydrol. Earth Syst. Sci. 20 (10) (2016) 4005–4015.
[32] F. Tauro, F. Tosi, S. Mattoccia, E. Toth, R. Piscopia, S. Grimaldi, Optical tracking velocimetry (OTV): leveraging optical flow and trajectory-based filtering for surface streamflow observations, Rem. Sens. 10 (12) (2018) 2010.
[33] F. Tosi, M. Rocca, F. Aleotti, M. Poggi, S. Mattoccia, F. Tauro, S. Grimaldi, Enabling image-based streamflow monitoring at the edge, Rem. Sens. 12 (12) (2020) 2047.
[34] A. Eltner, H. Sardemann, J. Grundmann, Flow velocity and discharge measurement in rivers using terrestrial and unmanned-aerial-vehicle imagery, Hydrol. Earth Syst. Sci. 24 (3) (2020).
[35] M.T. Perks, KLT-IV v1. 0: image velocimetry software for use with fixed and mobile platforms, Geosci. Model Dev. (GMD) 13 (12) (2020) 6111–6130.
[36] A. Dosovitskiy, P. Fischer, E. Ilg, P. Hausser, C. Hazirbas, V. Golkov, T. Brox, Flownet: learning optical flow with convolutional networks, Proceedings of the IEEE international conference on computer vision (2015) 2758–2766.
[37] E. Ilg, N. Mayer, T. Saikia, M. Keuper, A. Dosovitskiy, T. Brox, Flownet 2.0: evolution of optical flow estimation with deep networks, Proceedings of the IEEE conference on computer vision and pattern recognition (2017) 2462–2470.
[38] L. Fan, W. Huang, C. Gan, S. Ermon, B. Gong, J. Huang, End-to-end learning of motion representation for video understanding, Proceedings of the IEEE Conference on Computer Vision and Pattern Recognition (2018) 6016–6025.
[39] D. Sun, X. Yang, M.Y. Liu, J. Kautz, PWC-Net: CNNs for optical flow using pyramid, warping, and cost volume, Proceedings of the IEEE Conference on Computer Vision and Pattern Recognition (2018) 8934–8943.
[40] D.J. Butler, J. Wulff, G.B. Stanley, M.J. Black, A naturalistic open source movie for optical flow evaluation, in: European Conference on Computer *Vision*, Springer, *Berl*in, Heidelberg, 2012, October, pp. 611–625.
[41] S. Baker, D. Scharstein, J.P. Lewis, S. Roth, M.J. Black, R. Szeliski, A database and evaluation methodology for optical flow, Int. J. Comput. Vis. 92 (1) (2011) 1–31.
[42] D. Kondermann, R. Nair, K. Honauer, K. Krispin, J. Andrulis, A. Brock, B. Jahne, The hci benchmark suite: stereo and flow ground truth with uncertainties for urban autonomous driving, Proceedings of the IEEE Conference on Computer Vision and Pattern Recognition Workshops (2016) 19–28.
[43] M. Menze, A. Geiger, Object scene flow for autonomous vehicles, Proceedings of the IEEE conference on computer vision and pattern recognition (2015) 3061–3070.
[44] USGS, USGS 04087120 Menomonee River at Wauwatosa, WI. https://waterdata.usgs.gov/usa/nwis/uv?04087120, 2020. Accessed Jan 2020.
[45] DJI, "Matrice 2300 Series V2 Users Manual 1.4 (2019).
[46] K.H. Strobl, G. Hirzinger, in: More Accurate Pinhole Camera Calibration with Imperfect Planar Target, vol. 2011, IEEE International Conference on Computer Vision (ICCV), Barcelona, Spain, 2011, pp. 1068–1075. Nov 2011.

[47] J. Jyoti, H. Medeiros, S. Sebo, W. Mcdonald, Remote Sensing of River Velocity Using Drone Video and Optical Flow Algorithm. In*Watershed Management 2020*, American Society of Civil Engineers, Reston, VA, 2020, pp. 197–204.
[48] Y. LeCun, Y. Bengio, G. Hinton, Deep learning, nature 521 (7553) (2015) 436–444.
[49] K.M. Dawson-Howe, D. Vernon, Simple pinhole camera calibration, Int. J. Imag. Syst. Technol. 5 (1) (1994) 1–6.
[50] M. Detert, How to avoid and correct biased riverine surface image velocimetry, Water Resour. Res. 57 (2) (2021), e2020WR027833.
[51] K.F. Flynn, S.C. Chapra, Remote sensing of submerged aquatic vegetation in a shallow non-turbid river using an unmanned aerial vehicle, Rem. Sens. 6 (12) (2014) 12815–12836, https://doi.org/10.3390/rs61212815.
[52] Q.W. Lewis, B.L. Rhoads, LSPIV measurements of two-dimensional flow structure in streams using small unmanned aerial systems: 2. Hydrodynamic mapping at river confluences, Water Resour. Res. 54 (10) (2018) 7981–7999.
[53] P.J. Kinzel, C.J. Legleiter, sUAS-based remote sensing of river discharge using thermal particle image velocimetry and bathymetric lidar, Rem. Sens. 11 (19) (2019) 2317.

Jamir Shariar Jyoti received his MS in Electrical and Computer Engineering in 2020 from Marquette University and the B·Sc. degree from Khulna University of Engineering and Technology, Khulna, Bangladesh, in 2016. His Masters research work was mainly focused on computer vision and image processing-based applications in the area of water flow monitoring. He is currently working toward the Ph.D. degree with Electrical and Computer Engineering Department, Marquette University.

Henry Medeiros is an Associate Professor of Agricultural and Biological Engineering at the University of Florida. His research interests include computer vision and robotics with applications in areas such as manufacturing, agricultural automation, and public safety. He has published over fifty journal and peer-reviewed conference papers and holds several U.S. and international patents. He is a senior member of the IEEE and has been an associate editor for the IEEE International Conference on Robotics and Automation and the IEEE International Conference on Intelligent Robots. He received his Ph.D. from the School of Electrical and Computer Engineering at Purdue University.

Spencer Sebo received his MS in Environmental Engineering in 2020 from Marquette University. Spencer also holds a BS in Environmental Engineering Technology (2017) from the University of Wisconsin – Green Bay and a BS in Wildlife Ecology (2014) from the University of Wisconsin – Madison. His research focuses on sanitary sewer flow monitoring and identifying rainfall derived inflow and infiltration in sanitary sewer systems.

Dr. Walter McDonald is an assistant professor in the Civil, Construction and Environmental Engineering department at Marquette University. Dr. McDonald obtained a PhD in Civil Engineering from Virginia Tech in 2016 and holds a MS in Civil Engineering (2012) from Texas A&M University and a BS in Civil Engineering (2010) from Texas Tech University. His research integrates an innovative span of environmental monitoring, urban stormwater management, and data analytics. Specific projects include drone remote sensing of hydrologic processes, monitoring stormwater best management practices, and real-time control of stormwater systems.